ENVIRONMENTAL RESEARCH
LETTERS

PURPOSE-LED PUBLISHING™ Part of the ENVIRONMENTAL RESEARCH SERIES

LETTER • OPEN ACCESS

Alkalinity enhancement in subduction regions and the global ocean: efficiency, earth system feedbacks, and scenario sensitivity

To cite this article: Tanvi Nagwekar *et al* 2026 *Environ. Res. Lett.* **21** 014031

ENVIRONMENTAL RESEARCH
LETTERS

LETTER

Alkalinity enhancement in subduction regions and the global ocean: efficiency, earth system feedbacks, and scenario sensitivity

Tanvi Nagwekar[1,*], **Christopher Danek**[1], **Miriam Seifert**[1] and **Judith Hauck**[1,2]

[1] Alfred Wegener Institute Helmholtz Centre for Polar and Marine Research, Bremerhaven, Germany
[2] FB02 Biology/Chemistry, Universität Bremen, Bremen, Germany
[*] Author to whom any correspondence should be addressed.

E-mail: tanvi.nagwekar@awi.de

OPEN ACCESS

RECEIVED
29 October 2024

REVISED
25 November 2025

ACCEPTED FOR PUBLICATION
8 December 2025

PUBLISHED
9 January 2026

Keywords: ocean alkalinity enhancement, subduction regions, efficiency, earth system feedbacks, scenario sensitivity

Supplementary material for this article is available online

Abstract

Ocean alkalinity enhancement (OAE) refers to the addition of alkaline material to the surface ocean, which shifts carbonate chemistry towards more oceanic uptake of atmospheric CO_2. This study compares global OAE with regionally focused deployment in subduction regions of the Southern Ocean, Northwest Atlantic, and Norwegian-Barents Sea. We conducted ensemble simulations using an emissions-driven Earth System Model (ESM) under high- (SSP3-7.0) and low-emissions (SSP1-2.6) scenarios. By 2100, subduction region OAE was nearly as efficient (SSP3-7.0: 0.71 $\pm$ 0.03, SSP1-2.6: 0.60 $\pm$ 0.04) as global deployments (SSP3-7.0: 0.73 $\pm$ 0.01, SSP1-2.6: 0.64 $\pm$ 0.03). However, the ESM simulations did not reproduce the efficient vertical carbon transport seen in a previous ocean-only study, as strong internal variability and climate feedbacks to OAE hampered deep ocean carbon storage. The excess ocean CO_2 uptake and atmospheric CO_2 reduction were scenario-dependent (15%–19% and 22%–41% lower under SSP1-2.6 compared to SSP3-7.0, respectively). The pathways of excess ocean CO_2 uptake and atmospheric CO_2 reduction diverged between the scenarios after the mid-2060s, when atmospheric CO_2 peaked and then declined under SSP1-2.6, with a substantially larger relative land carbon loss in SSP1-2.6 than in SSP3-7.0 for regional OAE deployment. Furthermore, the emissions-driven ensemble simulations showed that climate feedbacks introduced substantial uncertainty in early decades of regional OAE efficiency, posing challenges for near-term monitoring, reporting, and verification. Reviewing our and previous model experiments revealed a strong linear relationship between added alkalinity and oceanic CO_2 uptake and atmospheric reduction, highlighting that first-order effects of OAE on carbonate chemistry are well understood and consistently represented, while the effects of carbon and climate feedbacks (13%–20%) and scenario sensitivity are smaller but non-negligible. Overall, our study shows that subduction regions can be a viable option for OAE; however, their efficiency is limited by these feedbacks and scenario sensitivity, which must be accounted for in future regional OAE interventions.

1. Introduction

The oceans are pivotal in regulating atmospheric CO_2 concentrations and have taken up about a quarter of the anthropogenic CO_2 emitted since preindustrial times (Gruber *et al* 2019, Friedlingstein *et al* 2025). One of the main drivers for oceanic carbon uptake and outgassing is alkalinity, defined as the excess of proton acceptors over donors in seawater (Zeebe and Wolf-Gladrow 2001, Wolf-Gladrow *et al* 2007). Naturally, land weathering processes deposit alkalinity in the surface ocean, shifting carbonate equilibria by converting dissolved CO_2 into bicarbonate and carbonate ions, which are not directly exchangeable with the atmosphere, aiding long-term carbon sequestration. The chemical shift lowers the partial pressure of CO_2 (pCO_2) at the ocean surface, enhancing oceanic CO_2 uptake (Hartmann *et al* 2013, Middelburg *et al* 2020). However, the current rate of oceanic CO_2 uptake due to natural land

weathering is almost two orders of magnitude lower than the anthropogenic CO_2 emission rates (Archer 2005), and thus cannot mitigate rising atmospheric CO_2 levels and global warming. Hence, in order to achieve the climate goal by the Paris Agreement to limit the global temperature increase to 2 °C above pre-industrial levels by 2100, drastic emissions reductions will likely need to be accompanied by efforts of various carbon dioxide removal (CDR) methods (UNFCCC 2015). Ocean alkalinity enhancement (OAE) is an ocean-based CDR method that can artificially elevate the rate of oceanic CO_2 uptake (Kheshgi 1995, Ilyina *et al* 2013, Keller *et al* 2014, Hauck *et al* 2016). This can be achieved by spreading alkaline powder or solutions from various sources, such as lime, olivine, basalt, calcium carbonate or hydroxide over the ocean surface (Caserini *et al* 2022).

Numerous modeling studies have explored OAE, yet the approach is still nascent (Babiker *et al* 2022). Currently the total CO_2 sequestration across novel CDR methods, including OAE, is estimated to be 0.00001–0.0002 MtC yr^{-1} (Friedlingstein *et al* 2025). Earth System Models (ESMs) demonstrate that OAE in high-emissions scenarios strengthens the ocean carbon sink, while the land carbon sink weakens due to atmospheric CO_2 reduction (Keller *et al* 2014, González and Ilyina 2016, Lenton *et al* 2018, Jeltsch-Thömmes *et al* 2024, Palmiéri and Yool 2024). Ocean-only models have also been used to explore OAE efficiencies in both global and regional applications, yielding varying results over the last decade after 75–80 years of deployment. For instance, Burt *et al* (2021) revealed region-dependent OAE efficiencies, with highest efficiencies in the sea-ice-free Southern Ocean and lowest in the subpolar North Atlantic. Contrarily, similar efficiencies were found for global OAE and OAE along ship-tracks (Köhler *et al* 2013), as well as for continuous OAE deployed globally and in the subduction regions of the Southern Ocean and North Atlantic (Nagwekar *et al* 2024). Notably, subduction regions could transfer a ∼2 times higher fraction of total carbon to the deep ocean compared to OAE in the global ocean (Nagwekar *et al* 2024). However, this contrasts with month-long pulsed OAE studies, which report low efficiencies in subduction regions due to low residence times of the water masses at the ocean surface and subsequent alkalinity loss to the deep ocean (Jones *et al* 2014, Bach *et al* 2023, He and Tyka 2023). Note that ocean-only models estimate the 'capture efficiency' of OAE due to prescribed atmospheric CO_2 and exclusion of climate feedbacks and thus tend to overestimate OAE efficiency globally and regionally compared to ESMs ('Earth System efficiency', Schwinger *et al* 2024).

Motivated by this discrepancy, this study quantifies the OAE efficiency of deep and bottom water formation regions in the Southern Ocean, Northwest Atlantic and Norwegian-Barents Sea region using a fully coupled, emissions-driven ESM for the 21st century. We assess whether the high regional efficiency previously identified in an ocean-only model (Nagwekar *et al* 2024) holds under a more comprehensive ESM setup that represents carbon and climate feedbacks. In doing so, we also consider how future emissions pathways influence the effectiveness of OAE in both regional and global deployments by simulating OAE under SSP1-2.6 (low-emissions, peak-and-decline) and SSP3-7.0 (high-emissions) scenarios. Furthermore, ensemble simulations are used to account for the often neglected uncertainty arising from internal climate variability in the ESM, which may pose a significant challenge for monitoring, reporting, and verification (MRV; Ho *et al* 2023) of OAE.

2. Methods

The simulations were carried out using the Alfred Wegener Institute ESM (AWI-ESM-1-REcoM, Danek *et al* 2023), based on the AWI Climate Model (AWI-CM1; Semmler *et al* 2020) but includes the ocean biogeochemistry model REcoM and incorporates dynamic vegetation (Hauck *et al* 2013, Schourup-Kristensen *et al* 2014; for details see Text S1). The ocean-circulation and biogeochemical components used in this study share the same initial conditions, horizontal resolution, carbonate chemistry routines, air–sea gas exchange coefficients, and KPP vertical mixing scheme as the ocean-only setup of Nagwekar *et al* (2024). The main difference is that the ocean-only configuration of Nagwekar *et al* (2024) uses FESOM2.1 with finite-volume numerical core (Koldunov *et al* 2019), coupled to the biogeochemical model REcoM3 with two phytoplankton and two zooplankton functional types (Gürses *et al* 2023). In contrast, the ESM used here employs FESOM1.4 with a finite-element numerical core (Wang *et al* 2014), coupled to REcoM2 with two phytoplankton and one zooplankton functional type. Importantly, the ESM also uses interactive rather than prescribed atmospheric CO_2, thereby allowing ocean–atmosphere interactions in response to a change in radiative forcing.

For this study, we start from a 970 year emissions-driven spinup under preindustrial forcing following the CMIP6 protocol (Eyring *et al* 2016), and branched three historical simulations, spaced 25 years apart, covering 1850–2014 following the C4MIP 'esm-hist' protocol (Jones *et al* 2016). These three ensemble members represent internal climate variability arising from distinct initial conditions. Subsequently, we conducted future scenario simulations (2015–2100) for each ensemble member under a high-emission (SSP3-7.0) and a low-emission (SSP1-2.6) pathway, following the C4MIP scenario protocol (Jones *et al* 2016; for details see Text S2), referred to as control (CTRL) simulations. The OAE simulations are branched off in 2030 from their

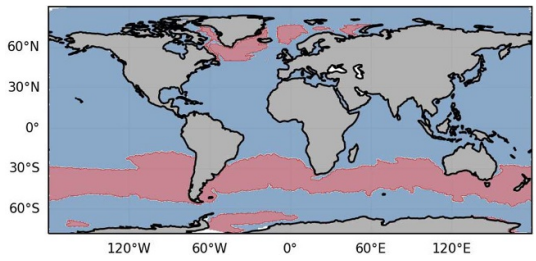

Figure 1. Red regions represent the alkalinity deposition mask for the subduction regions in the Southern Ocean, Northwest Atlantic and the Norwegian-Barents Sea region.

respective CTRL and are computed until the end of 2100.

We simulate the three ensemble members for global OAE (GLO-ALK) and subduction regions OAE (SUB-ALK; figure 1; for details see Text S3) with continuous and equal alkalinity addition per area (0.05 mol m^2 yr^{-1}) from 2030 to 2100. For GLO-ALK, 0.082 Pmol yr^{-1} of alkalinity is deposited (equivalent to 3 Pg yr^{-1} olivine deposition; Köhler *et al* 2013, Hauck *et al* 2016), which substantially exceeds the current global olivine production (0.0078–0.009 Pg yr^{-1} in 2018, Caserini *et al* 2022). In SUB-ALK, 0.018 Pmol yr^{-1} alkalinity is deposited (equivalent to 0.66 Pg yr^{-1} olivine). In both cases, added alkalinity is scaled with relative sea-ice cover in each grid cell and time-step, with no alkalinity addition in fully ice-covered cells. Hence, due to shrinking sea-ice cover towards the end of the century, 2.6% and 5.9% more alkalinity was added in the 2090s compared to the 2030s for global and regional OAE respectively, under SSP3-7.0 (table 1).

The OAE efficiency is calculated as the ratio of excess volume-integrated dissolved inorganic carbon (DIC) to excess volume-integrated alkalinity ($\eta CO_2 = \Delta DIC/\Delta Alk$; Renforth and Henderson 2017). It accounts for the accumulated increase in DIC and alkalinity relative to CTRL (Nagwekar *et al* 2024). In order to also consider carbon uptake and storage that occurs due to OAE but outside the regional deployment regions, we report efficiencies calculated from globally integrated ΔDIC and ΔAlk for GLO-ALK and SUB-ALK (table 1).

3. Results and discussion

3.1. Variability in the oceanic CO_2 uptake in response to OAE

Alkalinity perturbation globally and in the subduction regions enhances oceanic CO_2 uptake throughout the century compared to the CTRL simulation (figure 2(a)), although regional differences arise between ensemble members due to ocean–atmosphere interactions (figures 3(a)–(c)). In addition to the expected lower excess CO_2 uptake in SUB-ALK compared to GLO-ALK due to the lower amount of added alkalinity, we detect a substantial scenario uncertainty that varies over the course of the simulation and not uniformly across experiments (table 1). For SUB-ALK, the additional CO_2 uptake is lower by 18.8% in SSP1-2.6 than in SSP3-7.0 throughout the simulation. Notably, for GLO-ALK, the additional CO_2 uptake is higher in the 2030s (although within ensemble uncertainty), but lower in the 2090s in the low compared to the high-emissions scenario. All experiments, except GLO-ALK (SSP1-2.6), show increasing additional CO_2 uptake over time, driven by delayed ocean–atmosphere equilibration (Jones *et al* 2014, Bach *et al* 2023), elevated ocean carbonate chemistry sensitivity to enhanced alkalinity at the end of the century in a high-CO_2 world (Hauck *et al* 2016), and the increasing air–sea pCO_2 disequilibrium in SSP3-7.0 (Schwinger *et al* 2024). The GLO-ALK (SSP1-2.6) shows a slight decline in additional CO_2 uptake but remains within ensemble uncertainty (table 1).

The OAE efficiencies of GLO-ALK and SUB-ALK under the SSP3-7.0 scenario converge in the 2090s (0.71–0.73), which is in line with other OAE studies under a high emissions scenario using an ESM (e.g. 0.72–0.78; Feng *et al* 2017, Palmiéri and Yool 2024). We show that, in contrast to the high emissions scenario, the efficiencies under the SSP1-2.6 scenario are 12%–15% lower, ranging from 0.60 to 0.64 over the 2090s. This reduction is primarily due to the decreasing atmospheric CO_2 concentration under SSP1-2.6, which reduces the air–sea pCO_2 disequilibrium, along with a higher buffer capacity under SSP1-2.6, which decreases the sensitivity to alkalinity addition (Schwinger *et al* 2024).

Furthermore, regional OAE efficiency shows substantially higher uncertainty across its ensemble members in the first 20 years (SSP1-2.6: 38.4%; SSP3-7.0: 55.5%) than the global OAE experiments (SSP1-2.6: 5.9%; SSP3-7.0: 8.5%; figure 2(b)). This pronounced uncertainty in SUB-ALK is driven by differences in physical conditions across ensemble members. Variations in ocean temperature, circulation, and atmospheric forcing, particularly in parameters such as mixed layer depth (MLD), wind speed, and sea surface temperature (SST), which strongly regulate the air–sea CO_2 exchange, can lead to substantial fluctuations in regional carbon uptake (figure 3). Additionally, differences in sea-ice cover can influence the spatial extent of ice-free ocean available for alkalinity addition, altering both the magnitude and distribution of the perturbation. While similar physical variability occurs in the GLO-ALK ensemble members, the global distribution of alkalinity addition smooths out regional anomalies. In SUB-ALK, by contrast, the same physical variabilities among the ensemble members have a more pronounced impact because they are imposed on a smaller baseline flux. However, as the alkalinity anomaly is gradually redistributed by ocean circulation beyond the initial

Table 1. Amount of alkalinity added and response of the Earth System to the ocean alkalinity enhancement under the SSP3-7.0 and SSP1-2.6 emission scenarios. We report added alkalinity after scaling with sea-ice cover, excess of oceanic CO_2 uptake (ΔFCO_2), the efficiency metric ηCO_2 that is calculated as the volume-integrated excess dissolved inorganic carbon (DIC) over volume-integrated excess alkalinity over the global ocean, the cumulative changes in air–sea (ΔFCO_2 ocean cumulative) and air–land CO_2 flux (Δland CO_2 flux cumulative). We further list the increase in the DIC concentration in the top 1 km, below 1 km of the global ocean and percent of carbon stored below 1 km, changes in the atmospheric CO_2 mixing ratio and the surface air temperature (SAT; 2 m). The numbers are calculated as OAE experiment minus CTRL and are reported as an average over the 2030s, 2090s and the year 2100. Alkalinity added in the year 2100 represents the cumulative value.

Simulations	Alkalinity added [Pmol yr^{-1}]			ΔFCO_2 [PgC yr^{-1}]		ηCO_2 (ΔDIC/ΔAlk)		ΔFCO_2 ocean cumulative [PgC]		
				SSP3-7.0						
	2030s	2090s	2100 [Pmol]	2030s	2090s	2030s	2090s	2030s	2090s	2100
GLO-ALK	0.078	0.080	5.57	0.53 ± 0.09	0.75 ± 0.16	0.46 ± 0.05	0.73 ± 0.01	2.67 ± 0.21	45.28 ± 0.76	49.54 ± 0.74
SUB-ALK	0.017	0.018	1.28	0.13 ± 0.10	0.20 ± 0.15	0.38 ± 0.23	0.71 ± 0.03	0.59 ± 0.22	10.10 ± 0.51	11.21 ± 0.54
				SSP1-2.6						
GLO-ALK	0.078	0.078	5.51	0.62 ± 0.10	0.59 ± 0.09	0.52 ± 0.03	0.64 ± 0.03	3.10 ± 0.14	38.93 ± 1.56	41.76 ± 1.57
SUB-ALK	0.018	0.018	1.27	0.10 ± 0.10	0.19 ± 0.15	0.51 ± 0.24	0.60 ± 0.04	0.62 ± 0.21	8.42 ± 0.56	9.13 ± 0.62

Simulations	ΔDIC in top 1 km [PgC]			ΔDIC below 1 km [PgC]			ΔDIC below 1 km [%]		
				SSP3-7.0					
	2030s	2090s	2100	2030s	2090s	2100	2030s	2090s	2100
GLO-ALK	2.08 ± 0.45	41.27 ± 0.77	45.32 ± 1.29	0.11 ± 0.55	1.32 ± 0.50	1.16 ± 0.72	5.02 ± 35.8	3.10 ± 1.4	2.50 ± 1.9
SUB-ALK	0.26 ± 0.32	9.50 ± 1.00	10.23 ± 1.49	0.19 ± 0.25	-0.084 ± 0.93	0.27 ± 1.79	42.22 ± 43.9	-0.89 ± 12.0	2.57 ± 20.3
				SSP1-2.6					
GLO-ALK	2.58 ± 0.25	34.90 ± 1.34	37.06 ± 1.46	0.17 ± 0.24	1.51 ± 0.48	2.20 ± 0.82	6.18 ± 13.4	4.15 ± 1.5	5.60 ± 2.5
SUB-ALK	0.81 ± 0.23	8.04 ± 0.53	8.64 ± 0.33	-0.13 ± 0.20	-0.21 ± 1.20	0.065 ± 0.85	-19.1 ± 47.9	-2.68 ± 20.4	0.75 ± 12.8

Simulations	ΔLand carbon cumulative [PgC]			ΔAtmospheric CO_2 [ppm]			ΔSAT [°C]		
				SSP3-7.0					
	2030s	2090s	2100	2030s	2090s	2100	2030s	2090s	2100
GLO-ALK	-0.14 ± 2.10	-4.17 ± 2.66	-3.56 ± 3.39	-0.77 ± 0.64	-18.57 ± 0.99	-20.43 ± 0.59	0.005 ± 0.066	-0.053 ± 0.092	-0.043 ± 0.18
SUB-ALK	-1.44 ± 3.11	-0.73 ± 2.64	-1.99 ± 3.0	0.28 ± 0.95	-4.35 ± 0.89	-3.6 ± 1.12	0.01 ± 0.088	-0.016 ± 0.076	-0.054 ± 0.053
				SSP1-2.6					
GLO-ALK	-3.32 ± 1.1	-11.2 ± 4.70	-9.29 ± 5.1	0.19 ± 0.35	-12.43 ± 1.57	-14.67 ± 2.08	0.027 ± 0.057	-0.13 ± 0.10	-0.062 ± 0.022
SUB-ALK	-0.64 ± 1.30	-4.58 ± 2.31	-3.45 ± 1.74	0.17 ± 0.38	-1.83 ± 1.06	-2.25 ± 1.21	0.011 ± 0.071	-0.027 ± 0.11	0.069 ± 0.11

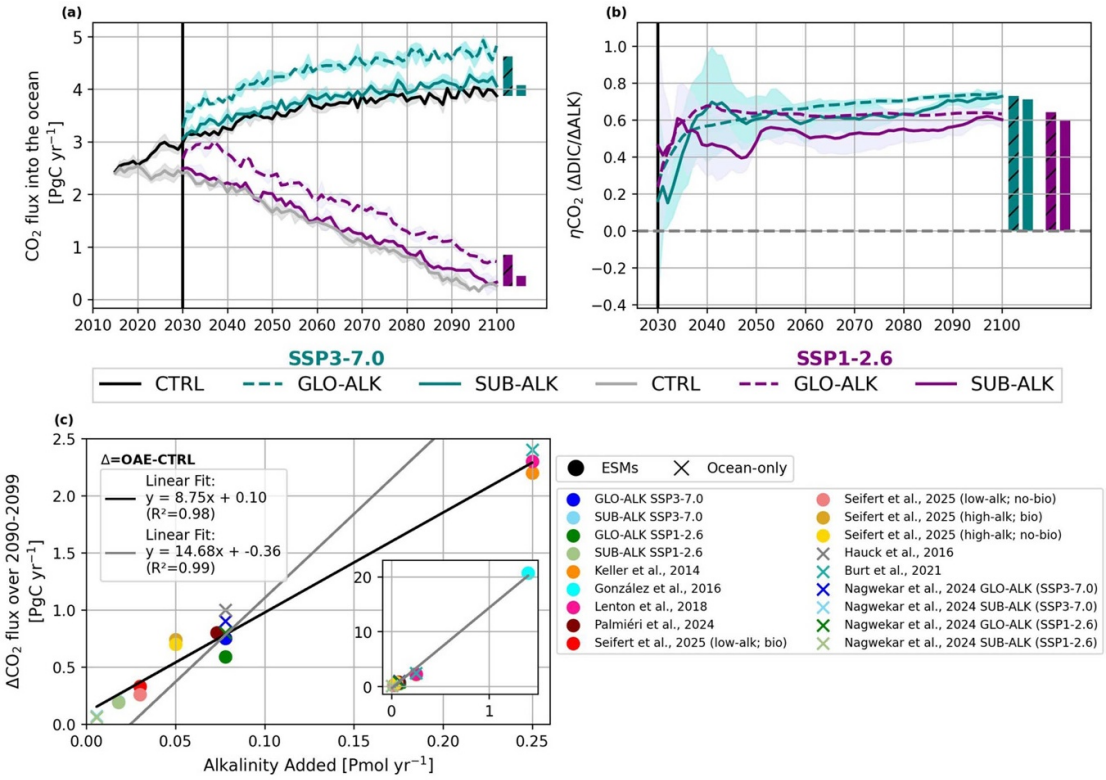

Figure 2. Globally integrated a) ocean CO_2 uptake and b) OAE efficiency ηCO_2 (volume-integrated increase in dissolved inorganic carbon divided by the volume-integrated increase in alkalinity relative to CTRL) in global (GLO-ALK; dashed lines) and subduction region (SUB-ALK; solid lines) OAE experiments for SSP3-7.0 (green) and SSP1-2.6 (purple) scenarios. Shading shows standard deviation over ensemble members. Bars show mean differences over 2090-2099 relative to CTRL for SUB-ALK (plain bars) and GLO-ALK (hatched bars). c) Increase in oceanic CO_2 uptake relative to CTRL versus added alkalinity averaged over 2090–2099. Solid gray (black) line shows linear fit over previous study results using ocean-only and ESMs in high- and low-emissions scenarios including (excluding) González and Ilyina (2016). For SUB-ALK, the markers for the SSP1-2.6 and SSP3-7.0 simulations differ only slightly and therefore overlap entirely (for both ocean-only model (Nagwekar *et al* 2024): crosses, and the ESM used here: dots).

regions of addition, the influence of local variability diminishes, leading to a reduction in ensemble spread over time for SUB-ALK. Given that the early decades are critical for real-world deployment, such high variability in regional OAE efficiency during this period can pose a substantial challenge for MRV. In comparison, ocean-only model studies that do not include coupled feedbacks have reported higher efficiencies, ranging from 0.85–0.95 for both global and regional OAE following the larger OAE-induced ocean CO_2 uptake (Köhler 2020, Burt *et al* 2021, He and Tyka 2023, Wang *et al* 2023, Nagwekar *et al* 2024). When comparing our simulations with ocean-only simulations from Nagwekar *et al* (2024), carbon feedbacks reduced the efficiency by 14% and 16.5% under SSP3-7.0, with stronger reductions of 19% and 24% under SSP1-2.6 for global and regional OAE, respectively. Moreover, the scenario sensitivity is larger in our ESM simulations where the efficiency is reduced by 12%–15% under SSP1-2.6 as compared to SSP3-7.0. In contrast, the ocean-only simulations have a smaller reduction of 7.1% due to the absence of an interactive carbon cycle. Despite the higher computational costs, the ESM explicitly represents carbon and carbon–climate feedbacks, thereby helping to elucidate the effect of these feedbacks on OAE outcomes.

The CO_2 uptake change scales linearly with the amount of added alkalinity, as also seen in other ESMs and ocean-only models (figure 2(c)). This mirrors the fact that the effect of OAE on ocean carbonate chemistry is well understood and uniformly represented across ESMs and ocean-only models. For instance, when adding as much alkalinity as in our GLO-ALK experiment to coastlines globally, the OAE-induced excess CO_2 uptake is comparable to our SSP3-7.0 emission scenario simulation (0.8 PgC yr^{-1}, Palmiéri and Yool 2024). Acknowledging existing gaps in the representation of abiotic feedbacks to alkalinity addition, this implies that the regional differences, carbon and climate feedbacks, and scenario sensitivity are dwarfed relative to the scaling of the oceanic CO_2 uptake change by the added amount of alkalinity. Accordingly, higher alkalinity deposition globally or regionally (0.25 and 1.4 Pmol yr^{-1}) results in proportionally higher excess CO_2 uptake (Ilyina *et al* 2013, Keller *et al* 2014, González and Ilyina 2016, Sonntag *et al* 2018). The comparison further confirms that the ocean-only models show higher excess CO_2 uptake than ESMs for the same alkalinity addition

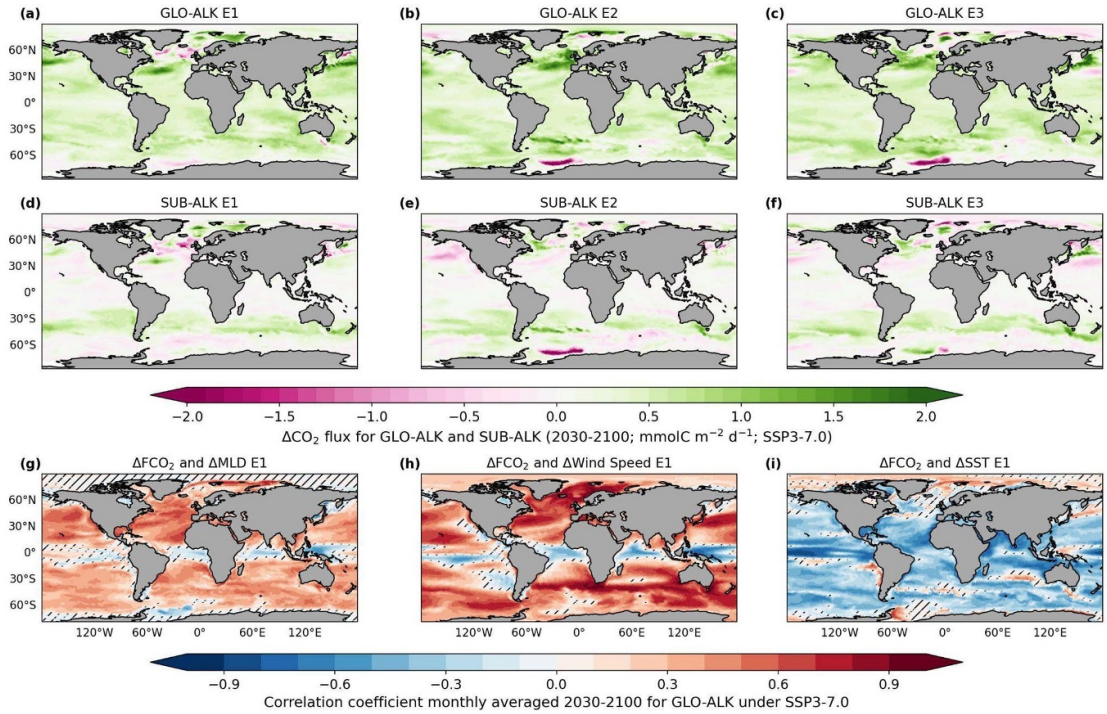

Figure 3. Spatial patterns for changes in the air–sea CO_2 flux relative to CTRL (ΔFCO_2) for each ensemble member averaged over 2030–2100 under SSP3-7.0 in (a)–(c) GLO-ALK and (d)–(f) SUB-ALK. CO_2 flux in CTRL is positive for uptake and negative for outgassing. In the ΔFCO_2 maps, positive indicates an increase in FCO_2 relative to CTRL and negative indicates a decrease in FCO_2 relative to CTRL. Correlation coefficients for GLO-ALK of the first ensemble member (E1) between ΔFCO_2 and (g) mixed layer depth (MLD) anomalies, (h) wind speed anomalies and (i) sea surface temperature (SST) anomalies, respectively. The hatched regions show where the correlation coefficient is not statistically significant (confidence level = 0.95). All correlations are calculated from monthly means over 2030–2100. See supplement figures S3 and S4 for the correlation patterns in other ensemble members of GLO-ALK and SUB-ALK under SSP3-7.0 and supplement figures S5, S6, and S7 for SSP1-2.6.

(figure 2(c)). For example, under both high- and low-emissions scenarios, depositing 0.078 Pmol yr^{-1} of alkalinity globally using an ocean-only setup increased the CO_2 uptake by 0.8–1.0 PgC yr^{-1} (Hauck *et al* 2016, Nagwekar *et al* 2024), which is 0.1–0.2 PgC yr^{-1} higher than in the emissions-driven ESM simulation GLO-ALK. Similarly, Burt *et al* (2021), using an ocean-only model with the same alkalinity addition (0.25 Pmol yr^{-1}; 2020–2100) as in the ESM studies of Keller *et al* (2014) and Lenton *et al* (2018), reported a slightly higher CO_2 uptake by 0.1 PgC yr^{-1} compared to the ESM studies. This difference is attributed to carbon and climate feedbacks in the ESMs and thus confirms that ocean-only studies provide an upper limit estimate of the increase in excess CO_2 uptake (Schwinger *et al* 2024).

In an ocean-only setup, global and subduction regions OAE revealed nearly uniform spatial patterns of CO_2 flux changes relative to CTRL (ΔFCO_2), with consistent positive anomalies (i.e. higher uptake) under both emission scenarios (Nagwekar *et al* 2024). In contrast, ESM simulations display more regional heterogeneity in ΔFCO_2, with negative anomalies locally (FCO_2 lower in OAE than in CTRL, i.e. lower uptake) caused by climate feedbacks under both scenarios (figures 3(a)–(f); supplement figure S5). Consequently, each ensemble member exhibits distinct regional patterns due to specific land–ocean–atmosphere interactions. For instance, in SUB-ALK, positive ΔFCO_2 (FCO_2 higher in OAE than in CTRL) occurs predominantly in the Southern Ocean, where we deposit alkalinity, but the Weddell Sea response varies across ensemble members. The North Atlantic also shows ensemble-member dependent results, with the first ensemble member in SUB-ALK exhibiting a negative ΔFCO_2, while the other two ensemble members show a positive anomaly (figures 3(d)–(f)). This response is likely linked to the variable deep mixing in these regions. In summary, these experiments illustrate how the spatial CO_2 flux response to OAE is modified by internal climate variability and land–ocean–atmosphere interactions.

The differences of CO_2 flux anomalies between ensemble members can be explained through well-known drivers of air–sea CO_2 fluxes (Takahashi *et al* 2009) that seemingly vary between ensemble members. Here, we illustrate this through maps of correlations between CO_2 flux anomalies with MLD (as a proxy for mixing), wind speed (one of the major drivers of gas-exchange) and SST anomalies (as a proxy for solubility). We find significant correlations throughout most of the global ocean (figures 3(g)–(i)) that are robust across ensemble members (figure S3-S7). Higher CO_2 uptake in

response to OAE occurs when the MLD is shallower, wind speeds are stronger, and SST is lower compared to the CTRL.

In our comparison, we argue that the crucial distinction in the models used is not the specific ocean or biogeochemical model version (FESOM2.1–REcoM3 in Nagwekar *et al* (2024) versus FESOM1.4–REcoM2 coupled to ECHAM–JSBACH in the ESM used here), but the fact that only the ESM includes an interactive atmosphere and land surface with freely evolving atmospheric CO_2 and allows for ocean–atmosphere interactions in response to altered radiative forcing (Fedorov 2009, Oschlies 2009). Likewise, comparing various different models, model-structural differences appear to be of secondary importance for the metrics analyzed here. To first order and on the spatiotemporal scales considered here, the simulated OAE response scales with the amount of alkalinity addition in both our ocean-only and ESM studies and other OAE studies (figure 2(c)), and dependence on the specific biogeochemical module is small because the signal is dominated by carbonate chemistry and almost all studies employ near-identical carbonate-system solvers (Friedlingstein *et al* 2025). Differences among ocean circulation models likely also lead to only modest differences for the predominantly surface-driven OAE response, especially on large temporal and spatial scales, acknowledging the potentially important differences in simulated mixed-layer depth, particularly on smaller temporal and regional scales. Consequently, the primary cause of the deviations between ocean-only and ESM OAE outcomes is the interactive ocean–atmosphere–land carbon cycle and the physical ocean–atmosphere interactions in response to changes in radiative forcing via OAE: (i) carbon feedbacks lead to lower globally integrated OAE-induced CO_2 flux anomalies and efficiencies in ESMs compared to models with prescribed atmospheric CO_2 (ocean-only models or atmospheric CO_2 concentration-driven ESMs, Oschlies 2009, Schwinger *et al* 2024); (ii) carbon–climate feedbacks act through radiatively driven changes in mixed-layer depth, winds, SST, and the freshwater cycle and, together with the carbon feedback, thus generate the spatially patchy CO_2 uptake anomalies and a wide ensemble spread seen in the ESM simulations.

3.2. Long-term carbon storage in form of dissolved inorganic carbon

With regard to changes in the DIC inventory (ΔDIC), the additional DIC in the top 1 km of the ocean scales between the GLO and SUB experiments with the amount of alkalinity added (table 1), but is lower in the low (GLO-ALK: 34.9 $\pm$ 1.34 PgC; SUB-ALK: 8.04 $\pm$ 0.53 PgC) than in the high-emission scenario (GLO-ALK: 41.3 $\pm$ 0.8 PgC; SUB-ALK:9.5 $\pm$ 1.0 PgC). Carbon accumulation due to OAE is positive throughout the top 1 km, with low interannual variability and ensemble spread (figure 4(a)). Below 1 km, ΔDIC shows high annual fluctuations and variability across ensemble members, with lower accumulation than CTRL during certain decades (figure 4(b)). This variability on a global and regional scale arises from climate feedbacks to OAE and internal climate variability in the ESM. The role of climate feedbacks is evident by SUB-ALK transferring, on average, a relative 8.4 times more excess carbon below 1 km than GLO-ALK in the 2030s (SSP3-7.0), but accumulated less excess carbon below 1 km in the 2090s with large variability across the ensemble. Under SSP1-2.6, SUB-ALK has negative ΔDIC below 1 km throughout most of the simulation period indicating a larger carbon redistribution than addition through OAE. In an ocean-only setup without climate feedbacks, SUB-ALK transferred a $\sim$2 times higher fraction of the total carbon uptake to the deep ocean than GLO-ALK (2090s, both emission scenarios, Nagwekar *et al* 2024). The carbon redistribution in the water column could, in principle, be sensitive to the choice of ocean circulation model when comparing the ocean-only simulations from Nagwekar *et al* (2024) with the ESM used here. However, the strongly divergent responses across the three ESM ensemble members for both GLO- and SUB-ALK suggest that such structural differences are not the dominant factor responsible. Instead, the contrast with the ocean-only results is most plausibly linked to carbon–climate feedbacks and the associated internal variability arising from ocean–atmosphere interactions (also see section 3.1). The internal climate variability is depicted by the fact that for one of the ensemble members under SSP3-7.0, SUB-ALK accumulates relatively more carbon than GLO-ALK in the 2090s, whereas the other two ensemble members show the opposite. This illustrates that without ensemble simulations, the large impact of internal climate variability on deep ocean carbon storage would be overlooked.

Along with temporal variability, ΔDIC also exhibits spatial variability (figures 4(c)–(f)). Positive ΔDIC occurs in the top 1 km, with maximum accumulation in the sub-tropical gyres and the Arctic, for both emissions scenarios. Below 1 km, ΔDIC increases prominently in the North Atlantic and along the Antarctic coast (figures 4(d) and (f)). Surprisingly, some negative ΔDIC anomalies also occur in the surface ocean. As this is not found in the ocean-only simulations, this must be driven by climate feedbacks that leads to redistribution of DIC within the water column. Possible processes that may play a role in these feedbacks are altered ocean circulation, mixing, biological productivity in the euphotic zone, and shifts of ocean fronts (Doney *et al* 2009, Clement and Gruber 2018, Keppler *et al* 2023). These confounding effects present a challenge for MRV if they rely on local measurements of changes in DIC and alkalinity inventories due to OAE. While

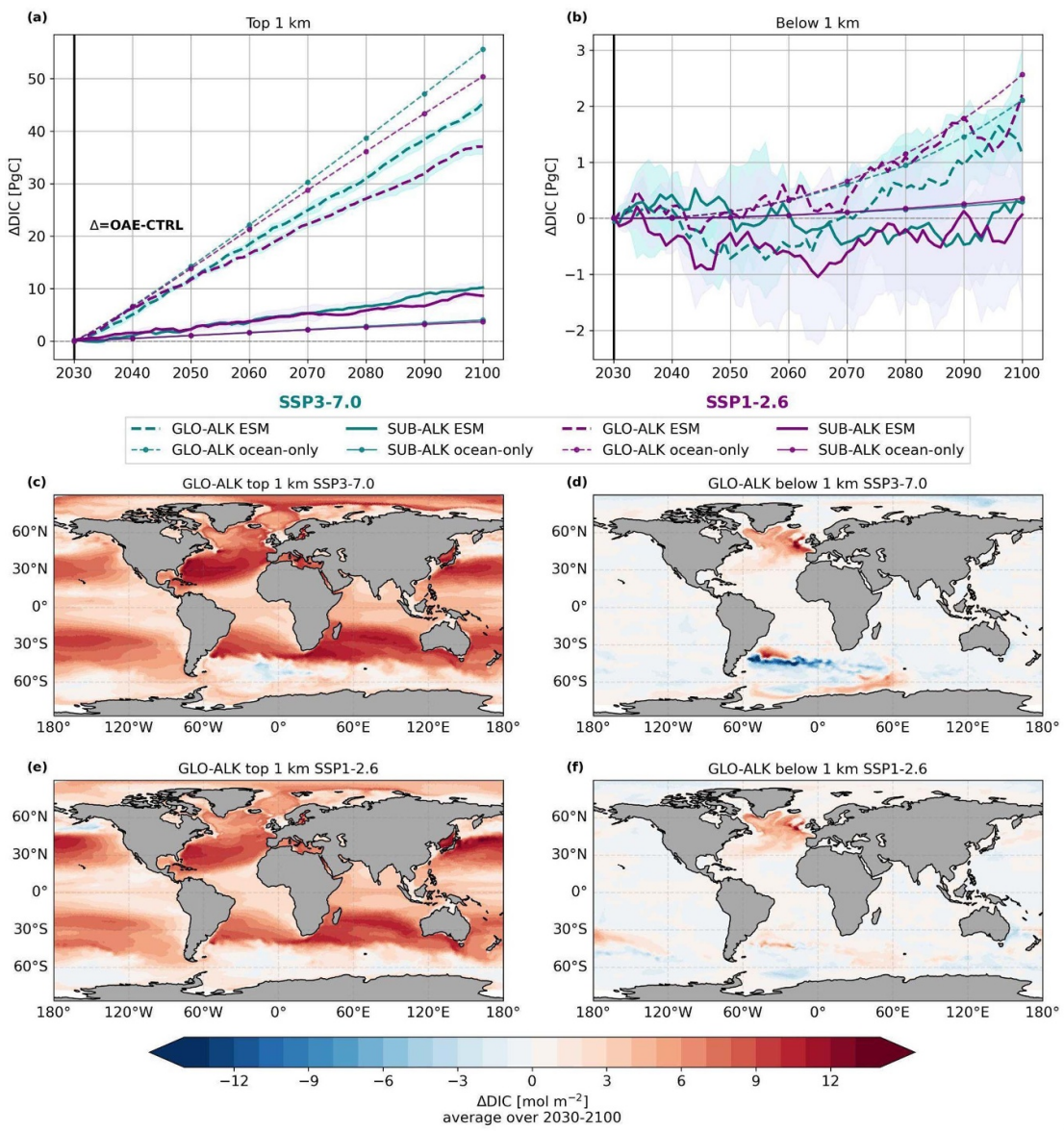

Figure 4. Volume-integrated dissolved inorganic carbon (DIC) relative to CTRL under SSP3-7.0 (green) and SSP1-2.6 (purple) emissions scenarios (a) in the top 1 km and (b) below for global OAE (GLO-ALK; dashed lines) and subduction regions OAE (SUB-ALK; solid lines). Lines without (with) circle markers represent ESM (ocean-only; Nagwekar *et al* 2024) simulations. Shading represents standard deviation of ensemble members. (c)–(f) Depth-integrated ΔDIC in GLO-ALK relative to CTRL using the ESM in the top 1 km and below under the SSP3-7.0 and SSP1-2.6 scenarios. See supplementary figures S8 and S9 for ΔDIC of individual ensemble members of GLO-ALK and SUB-ALK under SSP3-7.0 (supplementary figure S10 and S11 for SSP1-2.6). The soild and dashed lines with circle marks (ΔDIC for GLO-ALK and SUB-ALK under SSP1-2.6 and SSP3-7.0 emission scnearios) in (a), (b) are reproduced from Nagwekar *et al* (2024). CC BY 4.0.

model-based approaches inherently account for the uptake and subsequent redistribution or outgassing of carbon, point-based observational methods risk capturing only the localized drawdown signal while missing compensatory decreases elsewhere in the DIC inventory.

3.3. Impact of OAE on atmospheric CO_2, surface air temperature (SAT) and land carbon fluxes

A crucial outcome of OAE for climate change mitigation is the atmospheric CO_2 reduction. GLO-ALK and SUB-ALK reduce atmospheric CO_2 by 20.4 ± 0.6 ppm and 3.6 ± 1.1 ppm, respectively, in 2100 under SSP3-7.0 (figure 5(a)). The reduction in atmospheric CO_2 is substantially lower under SSP1-2.6 with a reduction of 14.7 ± 2.1 ppm (GLO-ALK) and 2.3 ± 1.2 ppm (SUB-ALK; figure 5(a); table 1). This is because under the SSP1-2.6 emission scenario, the background atmospheric CO_2 concentration peaks in the mid-2060s and decreases thereafter. The effect of OAE depends on the emissions pathway, with the efficiency reducing after the atmospheric CO_2 concentration peaks and thus, the air–sea disequilibrium decreases (Schwinger *et al* 2024). Such emissions scenario dependency thus becomes crucial in order to determine realistic carbon removal

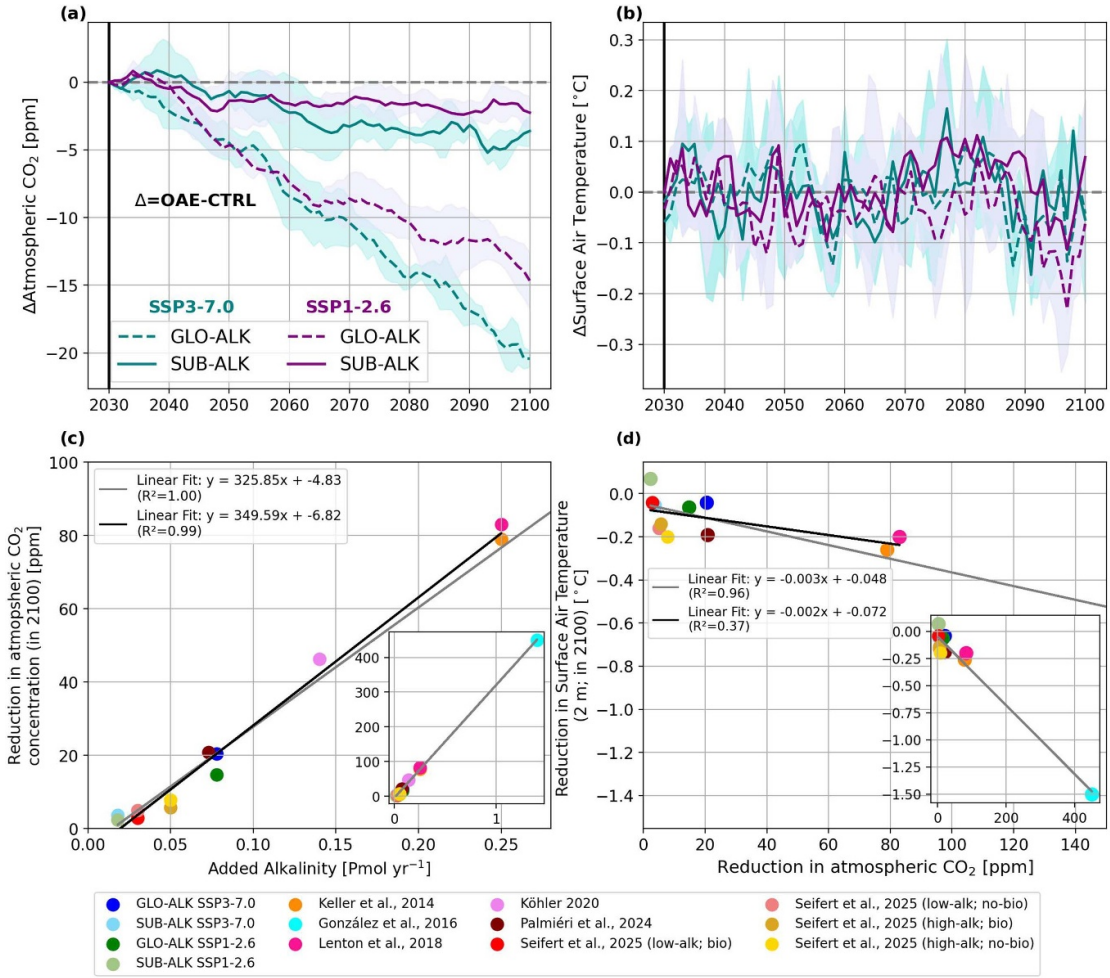

Figure 5. Time series for the change in (a) atmospheric CO_2 and (b) surface air temperature relative to the CTRL in global OAE (GLO-ALK; dashed lines) and subduction region OAE (SUB-ALK; solid lines) under SSP3-7.0 (green) and SSP1-2.6 (purple) emissions scenarios. Shades around the lines represent the standard deviation of the ensemble members. Scatter plots showing the relationship between (c) added alkalinity per year and the corresponding reduction in atmospheric CO_2 concentration in 2100, and (d) atmospheric CO_2 reduction and the decrease in surface air temperature (SAT; 2 m) across different studies using various Earth System Models. Solid gray (black) line shows linear fit over previous study results using ESMs in high- and low-emissions scenarios including (excluding) (González and Ilyina 2016). Data for SAT from Seifert *et al* (2025) was obtained via personal communication. In Seifert et al (2025), the term "bio" denotes simulations that consider the carbonate system effects on phytoplankton, whereas "no-bio" denotes simulations in which these effects are not considered.

efficiency and corresponding considerations for designing robust monitoring frameworks of OAE on a century long timescale.

The reduction in atmospheric CO_2 in 2100 under both emissions scenarios scales linearly with the added amount of alkalinity (figure 5(c), $R^2 = 1$). This linear relationship persists across various studies, despite differences in model configuration, resolution, and underlying assumptions, such as the region, period, method, and material used for OAE deployment. For example, Palmiéri and Yool (2024) simulated a decrease of 20.8 ppm in atmospheric CO_2 by 2100 from OAE along global coasts (0.078 Pmol yr^{-1}), which is comparable in terms of added alkalinity and CO_2 reduction to our GLO-ALK experiment under SSP3-7.0. This suggests a limited sensitivity of atmospheric CO_2 reduction to region of OAE deployment, consistent with findings by Lenton *et al* (2018), who reported a CO_2 reduction of 82–86 ppm for 0.25 Pmol yr^{-1} alkalinity addition globally and regionally by the end of the 21st century. Unlike the other studies, which apply a continuous alkalinity deployment method, Seifert *et al* (2025) implement a gradually increasing addition of alkalinity over the deployment period (2040–2100). They also account for carbonate system effects on phytoplankton, where elevated alkalinity can enhance coccolithophore calcification until substrate limitation constrains growth of all phytoplankton groups and coccolithophore calcification. For comparison in figure 5(c), we use the time-averaged alkalinity addition rate over the full deployment period from Seifert *et al* (2025). We find that neither the differing deployment scheme nor the inclusion of biological feedbacks have any substantial effect on the linear fit. We note, however, that no studies mentioned in figure 5(c) consider the secondary mineral precipitation or mineral dissolution effect of OAE (see

section 3.4). Further model development is needed to test if the linearity still holds when considering these processes.

Further, the atmospheric CO_2 reduction simulated in our experiments and in other studies is small compared to the historical atmospheric CO_2 increase due to fossil fuel emissions and land-use change. This re-emphasizes the need for drastic emissions reductions prior to application of negative emissions technologies. It is common sense that the human societies are more likely to achieve the climate targets and minimize negative impacts on marine ecology when applying OAE in low-emissions scenarios (Ho 2023). Yet, when only looking at ηCO_2 as the metric of OAE efficiency, OAE is 28.1% and 36.1% less effective in reducing atmospheric CO_2 for global and regional OAE, respectively, under the low-emissions scenario compared to the high-emissions scenario by 2100. Although most OAE modeling studies using an ESM are based on high-emissions scenarios, our results show that the atmospheric CO_2 reduction is not directly transferable between scenarios. Therefore, scenario dependency must be considered in climate policy decisions and the design of future mitigation pathways.

The atmospheric CO_2 reduction stimulated fluctuations in surface air temperature (SAT; 2 m). Compared to the CTRL simulation, SAT is reduced by a minor 0.053 ± 0.092 °C (GLO-ALK) and 0.016 ± 0.076 °C (SUB-ALK) in the 2090s under SSP3-7.0 and by 0.13 ± 0.10 °C (GLO-ALK) and 0.027 ± 0.11 °C (SUB-ALK) under the SSP1-2.6 emissions scenarios. The largest reduction occurs in GLO-ALK under SSP1-2.6, but all changes remain within the internal variability. In addition, the interannual variability is strong and SAT can at times also become higher than in the CTRL simulation. A comparison with other studies indicates that the response of SAT to atmospheric CO_2 reduction is highly model dependent (figure 5(d)). In contrast to the well understood carbon system response to OAE (figure 5(c)), the SAT signal depends on the model's equilibrium climate sensitivity (ECS). For instance, Palmiéri and Yool (2024) show a higher SAT reduction for a similar decrease in atmospheric CO_2 as our GLO-ALK under the high emissions scenario (figure 5(d)), due to the higher ECS of UKESM (5.4 °C; Sellar *et al* 2019) compared to AWI-ESM (3.3 °C; Semmler *et al* 2021). Further, a lag of approximately a decade in SAT response following CO_2 decline due to OAE has been reported (Jeltsch-Thömmes *et al* 2024). However, over a 70 years simulation, this lag probably has only a small effect. Our simulations under both emissions scenarios as well as previous studies under a high emissions scenario suggest that the scale of OAE applied (0.018–0.25 Pmol yr^{-1}) results in a negligible SAT decrease by 2100 (figure 5(d)). Thus, at this scale, OAE should be considered as part of a portfolio of other CDR techniques.

The total atmospheric carbon inventory is reduced by OAE, though a part of the enhanced ocean storage is compensated by a reduced land sink. For example, in GLO-ALK SSP3-7.0, the atmospheric carbon inventory in 2100 is reduced by 43.4 ± 1.3 PgC relative to CTRL, of which 49.5 ± 0.7 PgC are taken up by the oceans, but with a compensation of 7.3% or 3.6 ± 3.4 PgC by reduced land uptake (table 1). In GLO-ALK (SSP1-2.6), the total atmospheric carbon inventory is reduced by 31.2 ± 4.4 PgC, i.e. 28% less than in SSP3-7.0, which is due to a 16% weaker additional ocean carbon storage, but a 158% larger land carbon loss. Thus, under the low emissions scenario, the decreasing background atmospheric CO_2 concentration, after peaking in the 2060s, causes a relatively lower uptake of additional CO_2 by the oceans and a substantially stronger weakening of the land carbon sink. Together, these effects result in a higher retention of CO_2 in the atmosphere in response to global and regional OAE. In SUB-ALK (SSP1-2.6), up to 38% of the additional ocean carbon uptake is offset by the land sink (table 1), even though the absolute decrease in land uptake is similar between SSP1-2.6 and SSP3-7.0 and largely within their uncertainty ranges (figure 6(b)). This large fractional offset in SUB-ALK (SSP1-2.6) mainly reflects differences in additional ocean carbon uptake between SSP1-2.6 and SSP3-7.0 by the end of the century, due to the decline in background atmospheric CO_2 after the mid-2060s. Furthermore, it must be noted that the absolute decrease in land uptake is stronger in global than in regional OAE, however, in regional deployment, fluxes operate on smaller baseline ocean carbon fluxes, which may translate into a larger relative offset.

The divergences of the land carbon sink between the scenarios occurs in the mid 2060s, following the peak in atmospheric CO_2 in SSP1-2.6 (figure 6(b)), where the most pronounced absolute weakening of the land sink occurs in GLO-ALK (SSP1-2.6) and the largest weakening relative to the enhanced ocean sink occurs in the SUB-ALK (SSP1-2.6). In SUB-ALK, changes in the land carbon sink in SSP3-7.0 remain indistinguishable from zero throughout the 21st century, whereas a clear weakening emerges from 2060 for SSP1-2.6. In GLO-ALK, deviations from zero occur after 2080 in SSP3-7.0, indicating a time of emergence of around 50 years. Generally, OAE can affect the land carbon cycle through alterations in the atmospheric CO_2, SAT and precipitation. A reduction in atmospheric CO_2 diminishes the CO_2 fertilization effect, leading to a lower rate of carbon uptake by vegetation (Jeltsch-Thömmes *et al* 2024) and changes in the SAT and precipitation influence the vegetation dynamics and soil carbon storage (Adloff *et al* 2018). Previous studies have also reported a weakening of the land carbon sink in both global and regional

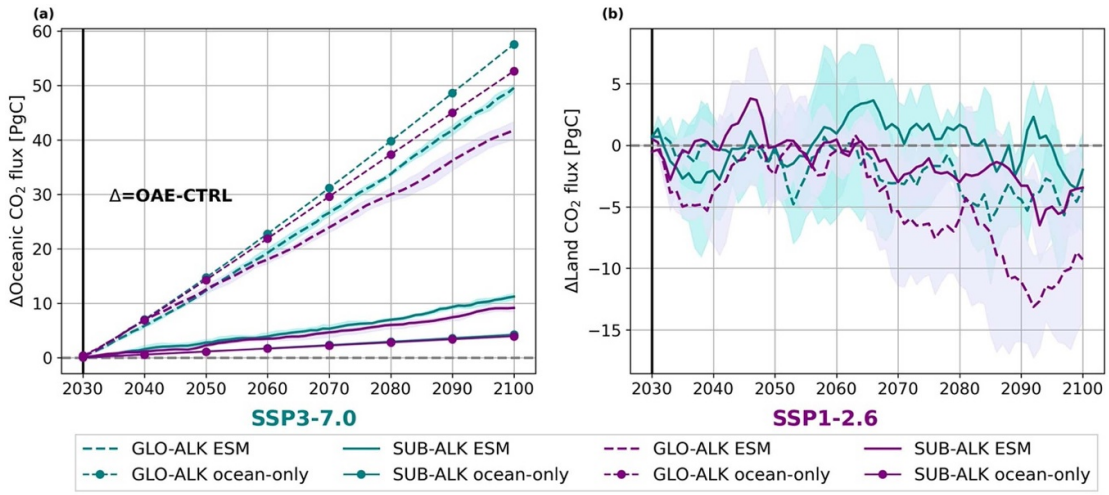

Figure 6. Time series for the cumulative change in (a) the oceanic CO_2 flux using the Earth System Model (ESM; without circular marker; this study) and ocean-only model (with circular marker; Nagwekar *et al* 2024) and (b) the land CO_2 flux changes using the ESM (this study) under SSP3-7.0 (green) and SSP1-2.6 (purple) emissions scenarios. Positive: strengthening of the carbon sinks. Both global OAE (GLO-ALK; dashed lines) and subduction region OAE (SUB-ALK; solid lines) are relative to the CTRL simulation. Lines from the ESM setup represent the ensemble mean and the shading is the standard deviation of the three ensemble members. Solid and dashed lines with cirle marker in (a) are reproduced from Nagwekar *et al* (2024).

OAE experiments (Keller *et al* 2014, González and Ilyina 2016, Lenton *et al* 2018, Palmiéri and Yool 2024). Here, we further show that this weakening is emission-scenario dependent for both global and regional OAE.

3.4. Limitations

We conducted idealized OAE experiments assuming instantaneous and complete dissolution of the added alkaline mineral in the surface ocean, in line with previous studies (Keller *et al* 2014, Hauck *et al* 2016, Lenton *et al* 2018, Butenschön *et al* 2021). An analogous outcome could be expected when alkalinity is added in aqueous form, as produced by reactor-based approaches (Eisaman *et al* 2023). In contrast, if powdered alkaline minerals are used instead, dissolution dynamics dependent on ambient seawater temperature, pH, and particle size becomes relevant. Previous studies show that dissolution is most efficient when finely ground minerals ($\sim$1 μm) are dissolved in warmer and more acidic waters (Köhler *et al* 2013, Feng *et al* 2017, Palmiéri and Yool 2024). However, observational data required to develop process-based parameterizations for dissolution and sinking rates in models remain scarce. Moreover, assuming that energy production is not fully decarbonized in the near term, this study neglects the energy costs associated with mining, grinding, transport, and distribution of solid minerals, which would lower the overall carbon removal efficiency.

Another unaddressed risk in our study is secondary calcium carbonate precipitation at high alkalinity concentrations, that may result in runaway precipitation and reduced OAE efficiency (Moras *et al* 2022, Hartmann *et al* 2023). Suitner *et al* (2024) observed runaway precipitation when aragonite saturation states (Ω_A) exceeded a threshold of 2.5–5.0. In another experiment, secondary precipitation drastically reduced the CDR potential from 0.8 to 0.1 mol CO_2 per mol alkalinity above an Ω_A threshold of $\sim$7 (Moras *et al* 2022). Our model simulations reached a maximum Ω_A value of 2.6–2.8 at individual surface grid points and months in the 2090s. Acknowledging that values at smaller time steps could be larger, this nevertheless suggests that critical levels of Ω_A are likely not widely reached in our global and regional OAE experiments.

While we added pure alkalinity to our model without accounting for potential biological effects, the different alkaline minerals used for OAE can differ considerably in terms of efficiency, and side effects on marine ecosystems. Reported effects include species-specific reduction in growth rates of diatoms and phytoplankton (Ferderer *et al* 2022, Guo *et al* 2022) and disruption of seafloor ecosystem due to sinking of undissolved alkaline mineral grains used for OAE (Feng *et al* 2017, Fuhr *et al* 2022). A model study that considers interactions between OAE and phytoplankton growth and calcification shows that indirect effects of alkalinity addition can decrease net primary production, and that changes in biological production and calcification have a small but non-negligible effect on OAE efficiency (Seifert *et al* 2025). While the study presents a first attempt to account for ecological consequences of OAE in a large-scale ocean model, field studies remain limited and the technology is in its infancy, leaving model projections sensitive to their choice of parameterizations. Therefore, targeted experiments and process studies are needed to constrain these parameterizations and improve model fidelity.

4. Conclusion

Our study confirms that OAE in subduction regions can be as efficient as OAE applied globally. However, the subduction regions are not as effective in transferring carbon to the deep ocean and the OAE efficiency in the ESM is lower compared to prior ocean-only simulations (Nagwekar *et al* 2024). This reduction of efficiency and deep carbon transfer is due to the influence of carbon and climate feedbacks and internal climate variability, which are represented in ESMs but absent in ocean-only frameworks. Ensemble simulations further reveal that this variability introduces considerable uncertainty in the initial two decades of regional OAE deployment. Since the initial phase is critical for real-world application, this early uncertainty can present challenges for MRV strategies that rely on model-based estimates or on only local observations.

The effectiveness of both global and regional OAE deployments depends on the underlying emissions scenario and the scenario sensitivity is underestimated in ocean-only models due to missing feedbacks. Under the low-emissions pathway SSP1-2.6, the gradual decline in atmospheric CO_2 concentrations after the mid-2060s reduces the air–sea pCO_2 disequilibrium. As this disequilibrium weakens, the ocean's uptake of additional carbon diminishes, thereby reducing the overall effectiveness of OAE. In our simulations, this scenario sensitivity led to 27.9% and 36.1% lower atmospheric CO_2 reductions for global (GLO-ALK) and regional (SUB-ALK) deployments, respectively, under SSP1-2.6 relative to SSP3-7.0. Importantly, the land carbon fluxes offset a relatively larger part of the enhanced oceanic uptake in the peak-and-decline scenario SSP1-2.6 than in the steadily increasing high-emission scenario and a larger part in the regional than in the global OAE experiment (up to 38%). These findings underline the importance of accounting for emissions scenario sensitivity when evaluating the performance of both global and regional OAE strategies.

A consistent linear relationship was observed between the amount of added alkalinity and both the reduction in atmospheric CO_2 and increase in oceanic CO_2 uptake. This linearity appears robust across models and provides a first-order estimate of OAE efficiency in the absence of currently unresolved processes such as secondary mineral precipitation and mineral dissolution kinetics. While this relationship is a useful guide for current-generation models, it also points to critical areas where future modeling efforts must improve by development of process parameterizations as observational constraints become available.

In conclusion, this study shows that while subduction regions can be viable for OAE, their efficiency is limited by internal climate variability, carbon and climate feedbacks, and sensitivity to emissions pathways. These factors must be considered in future model-based assessments and MRV strategies to ensure accurate quantification and evaluation of smaller scale regional OAE interventions.

Acknowledgment

This study was funded by Federal Ministry of Education and Research of Germany (BMBF) in the framework of RETAKE-B, one of the six research consortia of German Marine Research Alliance (DAM) research mission 'Marine carbon sinks on decarbonization pathways' (CDRmare); Grant: 03F0895B. JH and CD acknowledge funding by the Initiative and Networking Fund of the Helmholtz Association (Helmholtz Young Investigator Group Marine Carbon and Ecosystem Feedbacks in the Earth System [MarESys], Grant VH-NG-1301) and by the ERC-2022-STG OceanPeak (Grant 101077209). MS was funded by the European Union's Horizon 2020 research and innovation program under Grant Agreement No. 869357 (project OceanNETs). This work used resources of the Deutsches Klimarechenzentrum (DKRZ) granted by its Scientific Steering Committee (WLA) under Project ID ba1103. TN acknowledges support by the Open Access publication fund of Alfred-Wegener-Institut Helmholtz-Zentrum für Polar- und Meeresforschung. The work reflects only the author's view; the European Commission and their executive agency are not responsible for any use that may be made of the information the work contains. None of the authors have any competing interest.

Data availability statement

The data that support the findings of this study is available via zenodo: https://doi.org/10.5281/zenodo.17332931

ORCID iDs

Tanvi Nagwekar 0000-0002-6866-2508
Christopher Danek 0000-0002-4453-1140
Miriam Seifert 0000-0002-2570-5475
Judith Hauck 0000-0003-4723-9652

References

Adloff M, Reick C H and Claussen M 2018 Earth system model simulations show different feedback strengths of the terrestrial carbon cycle under glacial and interglacial conditions *Earth Syst. Dyn.* **9** 413–25

Archer D 2005 Fate of fossil fuel CO_2 in geologic time *J. Geophys. Res. Oceans* **110** C09S05

Babiker M *et al* 2022 Cross-sectoral perspectives *IPCC, 2022: Climate Change 2022: Mitigation Pathways Compatible with Long-term Goals* 1st edn, ed P R Shukla *et al* (Cambridge University Press) (https://doi.org/10.1017/9781009157926.005)

Bach L T, Ho D T, Boyd P W and Tyka M D 2023 Toward a consensus framework to evaluate air–sea CO_2 equilibration for marine CO_2 removal *Limnol. Oceanogr. Lett.* **8** 685–91

Burt D J, Fröb F and Ilyina T 2021 The sensitivity of the marine carbonate system to regional ocean alkalinity enhancement *Front. Clim.* **3** 624075

Butenschön M, Lovato T, Masina S, Caserini S and Grosso M 2021 Alkalinization scenarios in the mediterranean sea for efficient removal of atmospheric CO_2 and the mitigation of ocean acidification *Front. Clim.* **3** 614537

Caserini S, Storni N and Grosso M 2022 The availability of limestone and other raw materials for ocean alkalinity enhancement *Glob. Biogeochem. Cycles* **36** e2021GB007246

Clement D and Gruber N 2018 The eMLR(C*) method to determine decadal changes in the global ocean storage of anthropogenic CO_2 *Glob. Biogeochem. Cycles* **32** 654–79

Danek C, Gürses Ö, Gierz P, Andrés-Martínez M and Hauck J 2023 AWI AWI-ESM1REcoM model output prepared for CMIP6 C4MIP *Earth Syst. Grid Federation* (https://doi.org/10.22033/ESGF/CMIP6.17721)

Doney S C, Lima I, Feely R A, Glover D M, Lindsay K, Mahowald N, Moore J K and Wanninkhof R 2009 Mechanisms governing interannual variability in upper-ocean inorganic carbon system and air–sea CO_2 fluxes: physical climate and atmospheric dust *Deep Sea Res. II* **56** 640–55

Eisaman M D *et al* 2023 Assessing the technical aspects of ocean-alkalinity-enhancement approaches *State Planet* **2-oae2023** 1–29

Eyring V, Bony S, Meehl G A, Senior C A, Stevens B, Stouffer R J and Taylor K E 2016 Overview of the Coupled Model Intercomparison Project Phase 6 (CMIP6) experimental design and organization *Geosci. Model. Dev.* **9** 1937–58

Fedorov A 2009 *Ocean-atmosphere Coupling* (Oxford University Press)

Feng E Y, Koeve W, Keller D P and Oschlies A 2017 Model-based assessment of the CO_2 sequestration potential of coastal ocean alkalinization *Earth's Future* **5** 1252–66

Ferderer A, Chase Z, Kennedy F, Schulz K G and Bach L T 2022 Assessing the influence of ocean alkalinity enhancement on a coastal phytoplankton community *Biogeosciences* **19** 5375–99

Friedlingstein P *et al* 2025 Global carbon budget 2025 *Earth Syst. Sci. Data Discuss.* (https://doi.org/10.5194/essd-2025-659)

Fuhr M, Geilert S, Schmidt M, Liebetrau V, Vogt C, Ledwig B and Wallmann K 2022 Kinetics of olivine weathering in seawater: an experimental study *Front. Clim.* **4** 831587

González M F and Ilyina T 2016 Impacts of artificial ocean alkalinization on the carbon cycle and climate in Earth system simulations *Geophys. Res. Lett.* **43** 6493–502

Gruber N *et al* 2019 The oceanic sink for anthropogenic CO_2 from 1994 to 2007 *Science* **363** 1193–9

Guo J A, Strzepek R, Willis A, Ferderer A and Bach L T 2022 Investigating the effect of nickel concentration on phytoplankton growth to assess potential side-effects of ocean alkalinity enhancement *Biogeosciences* **19** 3683–97

Gürses Ö, Oziel L, Karakuş O, Sidorenko D, Völker C, Ye Y, Zeising M, Butzin M and Hauck J 2023 Ocean biogeochemistry in the coupled ocean–sea ice–biogeochemistry model FESOM2.1–REcoM3 *Geosci. Model. Dev.* **16** 4883–936

Hartmann J, Suitner N, Lim C, Schneider J, Marín-Samper L, Arístegui J, Renforth P, Taucher J and Riebesell U 2023 Stability of alkalinity in ocean alkalinity enhancement (OAE) approaches—consequences for durability of CO_2 storage *Biogeosciences* **20** 781–802

Hartmann J, West A J, Renforth P, Köhler P, De La Rocha C L, Wolf-Gladrow D A, Dürr H H and Scheffran J 2013 Enhanced chemical weathering as a geoengineering strategy to reduce atmospheric carbon dioxide, supply nutrients, and mitigate ocean acidification: ENHANCED WEATHERING *Rev. Geophys.* **51** 113–49

Hauck J, Köhler P, Wolf-Gladrow D and Völker C 2016 Iron fertilisation and century-scale effects of open ocean dissolution of olivine in a simulated CO_2 removal experiment *Environ. Res. Lett.* **11** 024007

Hauck J, Völker C, Wang T, Hoppema M, Losch M and Wolf-Gladrow D A 2013 Seasonally different carbon flux changes in the Southern Ocean in response to the southern annular mode *Glob. Biogeochem. Cycles* **27** 1236–45

He J and Tyka M D 2023 Limits and CO_2 equilibration of near-coast alkalinity enhancement *Biogeosciences* **20** 27–43

Ho D T, Bopp L, Palter J B, Long M C, Boyd P W, Neukermans G and Bach L T 2023 Monitoring, reporting, and verification for ocean alkalinity enhancement *State Planet* **2-oae2023** 1–12

Ho D 2023 Carbon dioxide removal is not a current climate solution — we need to change the narrative *Nature* **616** 9

Ilyina T, Wolf-Gladrow D, Munhoven G and Heinze C 2013 Assessing the potential of calcium-based artificial ocean alkalinization to mitigate rising atmospheric CO_2 and ocean acidification: MODELING MITIGATION POTENTIAL OF AOA *Geophys. Res. Lett.* **40** 5909–14

Jeltsch-Thömmes A, Tran G, Lienert S, Keller D P, Oschlies A and Joos F 2024 Earth system responses to carbon dioxide removal as exemplified by ocean alkalinity enhancement: tradeoffs and lags *Environ. Res. Lett.* **19** 054054

Jones C D *et al* 2016 Simulating the Earth system response to negative emissions *Environ. Res. Lett.* **11** 095012

Jones D C, Ito T, Takano Y and Hsu W-C 2014 Spatial and seasonal variability of the air-sea equilibration timescale of carbon dioxide *Glob. Biogeochem. Cycles* **28** 1163–78

Keller D P, Feng E Y and Oschlies A 2014 Potential climate engineering effectiveness and side effects during a high carbon dioxide-emission scenario *Nat. Commun.* **5** 3304

Keppler L, Landschützer P, Lauvset S K and Gruber N 2023 Recent trends and variability in the oceanic storage of dissolved inorganic carbon *Glob. Biogeochem. Cycles* **37** e2022GB007677

Kheshgi H S 1995 Sequestering atmospheric carbon dioxide by increasing ocean alkalinity *Energy* **20** 915–22

Köhler P 2020 Anthropogenic CO_2 of high emission scenario compensated after 3500 years of ocean alkalinization with an annually constant dissolution of 5 Pg of olivine *Front. Clim.* **2** 575744

Köhler P, Abrams J F, Völker C, Hauck J and Wolf-Gladrow D A 2013 Geoengineering impact of open ocean dissolution of olivine on atmospheric CO_2, surface ocean pH and marine biology *Environ. Res. Lett.* **8** 014009

Koldunov N V, Aizinger V, Rakowsky N, Scholz P, Sidorenko D, Danilov S and Jung T 2019 Scalability and some optimization of the finite-volumE sea ice–ocean model, version 2.0 (FESOM2) *Geosci. Model. Dev.* **12** 3991–4012

Lenton A, Matear R J, Keller D P, Scott V and Vaughan N E 2018 Assessing carbon dioxide removal through global and regional ocean alkalinization under high and low emission pathways *Earth Syst. Dyn.* **9** 339–57

Middelburg J J, Soetaert K and Hagens M 2020 Ocean alkalinity, buffering and biogeochemical processes *Rev. Geophys.* **58** e2019RG000681

Moras C A, Bach L T, Cyronak T, Joannes-Boyau R and Schulz K G 2022 Ocean alkalinity enhancement—avoiding runaway $CaCO_3$ precipitation during quick and hydrated lime dissolution *Biogeosciences* **19** 3537–57

Nagwekar T, Nissen C and Hauck J 2024 Ocean alkalinity enhancement in deep water formation regions under low and high emission pathways *Earth's Future* **12** e2023EF004213

Oschlies A 2009 Impact of atmospheric and terrestrial CO_2 feedbacks on fertilization-induced marine carbon uptake *Biogeosciences* **6** 1603–13

Palmiéri J and Yool A 2024 Global-scale evaluation of coastal ocean alkalinity enhancement in a fully coupled earth system model *Earth's Future* **12** e2023EF004018

Renforth P and Henderson G 2017 Assessing ocean alkalinity for carbon sequestration: ocean alkalinity for C sequestration *Rev. Geophys.* **55** 636–74

Schourup-Kristensen V, Sidorenko D, Wolf-Gladrow D A and Völker C 2014 A skill assessment of the biogeochemical model REcoM2 coupled to the finite element sea ice–ocean model (FESOM 1.3) *Geosci. Model. Dev.* **7** 2769–802

Schwinger J, Bourgeois T and Rickels W 2024 On the emission-path dependency of the efficiency of ocean alkalinity enhancement *Environ. Res. Lett.* **19** 074067

Seifert M, Danek C, Völker C and Hauck J 2025 Interactions between ocean alkalinity enhancement and phytoplankton in an Earth system model *Biogeosciences* **22** 5897–919

Sellar A A *et al* 2019 UKESM1: description and evaluation of the U.K. earth system model *J. Adv. Model. Earth Syst.* **11** 4513–58

Semmler T *et al* 2020 Simulations for CMIP6 with the AWI climate model AWI-CM-1-1 *J. Adv. Model. Earth Syst.* **12** e2019MS002009

Semmler T, Jungclaus J, Danek C, Goessling H F, Koldunov N V, Rackow T and Sidorenko D 2021 Ocean model formulation influences transient climate response *J. Geophys. Res. Oceans* **126** e2021JC017633

Sonntag S, Ferrer González M, Ilyina T, Kracher D, Nabel J E M S, Niemeier U, Pongratz J, Reick C H and Schmidt H 2018 Quantifying and comparing effects of climate engineering methods on the earth system *Earth's Future* **6** 149–68

Suitner N, Faucher G, Lim C, Schneider J, Moras C A, Riebesell U and Hartmann J 2024 Ocean alkalinity enhancement approaches and the predictability of runaway precipitation processes: results of an experimental study to determine critical alkalinity ranges for safe and sustainable application scenarios *Biogeosciences* **21** 4587–604

Takahashi T *et al* 2009 Climatological mean and decadal change in surface ocean pCO_2, and net sea–air CO_2 flux over the global oceans *Deep Sea Res. II* **56** 554–77

UNFCCC 2015 United Nations framework on climate change (UNFCCC): adoption of the Paris Agreement *21st Conference of the Parties* (available at: https://unfccc.int/sites/default/files/english_paris_agreement.pdf)

Wang H, Pilcher D J, Kearney K A, Cross J N, Shugart O M, Eisaman M D and Carter B R 2023 Simulated impact of ocean alkalinity enhancement on atmospheric co $_2$ removal in the bering sea *Earth's Future* **11** e2022EF002816

Wang Q, Danilov S, Sidorenko D, Timmermann R, Wekerle C, Wang X, Jung T and Schröter J 2014 The finite element sea ice-ocean model (FESOM) v.1.4: formulation of an ocean general circulation model *Geosci. Model. Dev.* **7** 663–93

Wolf-Gladrow D A, Zeebe R E, Klaas C, Körtzinger A and Dickson A G 2007 Total alkalinity: the explicit conservative expression and its application to biogeochemical processes *Mar. Chem.* **106** 287–300

Zeebe R E and Wolf-Gladrow D 2001 *CO_2 in Seawater: Equilibrium, Kinetics, Isotopes* (Gulf Professional Publishing)